Generation of hiPSC-derived low threshold mechanoreceptors containing axonal termini resembling bulbous sensory nerve endings and expressing Piezo1 and Piezo2

Shuyong Zhu [a,b,*], Nancy Stanslowsky [c], Jorge Fernández-Trillo [d], Tamrat M. Mamo [e], Pengfei Yu [a], Norman Kalmbach [c], Birgit Ritter [a], Reto Eggenschwiler [f,g], Werner J. D. Ouwendijk [h], David Mzinza [i], Likai Tan [i], Andreas Leffler [j], Michael Spohn [k], Richard J. P. Brown [l], Kai A. Kropp [a], Volkhard Kaever [m], Teng-Cheong Ha [n], Pratibha Narayanan [o], Adam Grundhoff [k], Reinhold Förster [b,i], Axel Schambach [n,p], Georges M.G.M. Verjans [h], Manuela Schmidt [o], Andreas Kispert [e], Tobias Cantz [f,g], Ana Gomis [d], Florian Wegner [c], Abel Viejo-Borbolla [a,b,*]

[a] *Institute of Virology, Hannover Medical School, Germany*
[b] *Cluster of Excellence-Resolving Infection Susceptibility (RESIST), Hannover Medical School, Germany*
[c] *Department of Neurology, Hannover Medical School, Germany*
[d] *Instituto de Neurociencias, Universidad Miguel Hernández-Consejo Superior de Investigaciones Científicas, Spain*
[e] *Institute of Molecular Biology, Hannover Medical School, Germany*
[f] *Research Group Translational Hepatology and Stem Cell Biology, Cluster of Excellence REBIRTH, Hannover Medical School, Germany*
[g] *Department of Gastroenterology, Hepatology and Endocrinology, Hannover Medical School, Germany*
[h] *Department of Viroscience, Erasmus Medical Center, the Netherlands*
[i] *Institute of Immunology, Hannover Medical School, Germany*
[j] *Department of Anesthesiology and Intensive Care Medicine, Hannover Medical School, Germany*
[k] *The Heinrich Pette Institute, Leibniz Institute for Experimental Virology, Germany*
[l] *Division of Veterinary Medicine, Paul-Ehrlich-Institute, Germany*
[m] *Research Core Unit Metabolomics, Institute of Pharmacology, Hannover Medical School, Germany*
[n] *Institute of Experimental Hematology, Hannover Medical School, Germany*
[o] *Max Planck Institute of Experimental Medicine, Germany*
[p] *Division of Hematology/Oncology, Boston Children's Hospital, Harvard Medical School, MA, USA*

ARTICLE INFO

ABSTRACT

Somatosensory low threshold mechanoreceptors (LTMRs) sense innocuous mechanical forces, largely through specialized axon termini termed sensory nerve endings, where the mechanotransduction process initiates upon activation of mechanotransducers. In humans, a subset of sensory nerve endings is enlarged, forming bulb-like expansions, termed bulbous nerve endings. There is no *in vitro* human model to study these neuronal endings. Piezo2 is the main mechanotransducer found in LTMRs. Recent evidence shows that Piezo1, the other mechanotransducer considered absent in dorsal root ganglia (DRG), is expressed at low level in somatosensory neurons. We established a differentiation protocol to generate, from iPSC-derived neuronal precursor cells, human LTMR recapitulating bulbous sensory nerve endings and heterogeneous expression of Piezo1 and Piezo2. The derived neurons express LTMR-specific genes, convert mechanical stimuli into electrical signals and have specialized axon termini that morphologically resemble bulbous nerve endings. Piezo2 is concentrated within these enlarged axon termini. Some derived neurons express low level Piezo1, and a subset co-express both channels. Thus, we

---

* Corresponding authors at: Institute of Virology, Hannover Medical School, Carl-Neuberg Strasse 1, 30625 Hannover, Germany.
E-mail addresses: zhu.shuyong@mh-hannover.de (S. Zhu), viejo-borbolla.abel@mh-hannover.de (A. Viejo-Borbolla).

generated a unique, iPSCs-derived human model that can be used to investigate the physiology of bulbous sensory nerve endings, and the role of Piezo1 and 2 during mechanosensation.

1. Introduction

Somatosensory neurons respond to mechanical stimuli from the environment and body, regulating touch, proprioception and pain, among others. Different somatosensory subtypes have distinct threshold mechanosensitivities (Delmas et al., 2011). Among them, low-threshold mechanoreceptors (LTMRs) mainly detect innocuous forces of low threshold range (Li et al., 2011). Dysfunction of LTMRs is associated with autism spectrum disorders (Tomchek and Dunn, 2007), and mechanical allodynia (Dhandapani et al., 2018). LTMRs are functionally, anatomically and morphologically heterogeneous, classified as Aβ-, Aδ- and C-LTMRs based on their axonal conduction velocity, soma size, axon diameter, and myelination degree (Abraira and Ginty, 2013). Upon mechanical activation, LTMRs convert force energy into mechanically-activated (MA) currents of different kinetics: rapidly (RA), intermediately (IA), and slowly adapting (SA) (Drew et al., 2002; Hao and Delmas, 2010; Lechner and Lewin, 2013).

Cutaneous LTMRs extend peripheral nerves into the skin. The termini of these nerves, termed sensory nerve endings, contain mechanotransducers that are force-gated ion channels (Iggo and Andres, 1982). In the skin, these terminal branches either end as free nerve endings or as mechanosensory end organs containing accessory cells such as Merkel cells, terminal glia or keratinocytes (Abraira and Ginty, 2013). In humans, a portion of the peripheral nerve endings that innervate Merkel cells and Meissner corpuscles are enlarged, forming bulb-like expansions (García-Mesa et al., 2017; Nolano et al., 2003; Nolano et al., 2008). Human mechanoreceptors innervating the scleral spur and mouse afferent nerve endings innervating Merkel cells are also enlarged (Tamm et al., 1994; Woo et al., 2014). However, mainly due to their inaccessibility *in vivo* (Delmas et al., 2011), the physiological relevance of the enlargement of these sensory nerve endings in humans, remains unknown. Thus, *in vitro* generation of human LTMRs with axonal termini resembling bulbous sensory nerve endings, using stem cell technology, may help to reveal the relevance of such enlarged structures.

Identification of Piezo1 and Piezo2 as mammalian mechanotransducers marks a milestone in mechanobiology (Coste et al., 2010). Piezo2 is the main functional mechanotransducer in human sensory neurons (Chesler et al., 2016), and required for mechanosensitivity in human stem cell-derived LTMR (Schrenk-Siemens et al., 2015). *In vivo*, Piezo2 locates at the soma (Ranade et al., 2014) and sensory nerve endings (Woo et al., 2014; García-Mesa et al., 2017). Piezo2 generates RA currents when expressed in HEK293T cells (Coste et al., 2010).

Piezo1 has an innate ability as a force transducer (Syeda et al., 2016). It is accepted that Piezo1 is mainly expressed in non-sensory neurons, due to its very low mRNA in mDRG (Coste et al., 2010). siRNA-mediated knockdown of Piezo1 in mDRG primary culture has negligible effects on RA current profiles, although results in slightly, but not significant, attenuated IA currents (Ranade et al., 2014). However, Piezo1 is functionally expressed in cultured human and mouse DRG neurons (Roh et al., 2020). Despite the low basal expression in mouse sensory neurons, Piezo1 suppresses axonal regeneration in response to injury, indicative of its functional activity (Song et al., 2019). There is no human stem cell-derived sensory neuronal model to study Piezo1 *in vitro*.

We established a robust differentiation protocol to generate human LTMRs-like neurons (termed SZ-LTMRs), from iPSCs-derived neuronal precursor cells that have multipotency and capability of self-renewal. The SZ-LTMRs express functional Piezo1 at a low level, and concentrate Piezo2 into their enlarged axon termini that morphologically mimic bulbous nerve endings found *in vivo*. Some of the SZ-LTMRs co-

express Piezo1 and Piezo2. We also detected Piezo1 mRNA in human sensory ganglia. We thus provide a unique, iPSC-based culture system to model the bulbous sensory nerve endings, and recapitulate the *in vivo* expression profiles of Piezo1 and Piezo2.

2. Materials and methods

2.1. smNPCs maintenance and differentiation

Maintenance: Previously generated smNPCs (Naujock et al., 2014) were grown on Matrigel (Corning, 354263) coated dishes, fed with N2/B27 medium containing 3 μM CHIR99021 (Axon Medchem, The Netherlands), 0.5 μM purmorphamine (PMA, Alexis, NY), and 150 μM L-Ascorbic acid (Sigma, A4403). The cells were fed every 2 days. Cells were detached by Accutase (MerckMillipore, SCR005, or PAA, *L*11-007) and split at a ratio of 1:6 for passaging. Unless otherwise noted, smNPCs at passages 59–62 were used in this study.

Differentiation: To induce peripheral sensory progenitors the maintenance medium was replaced with N2/B27 medium containing 10 μM CHIR9902 to activate WNT signalling, 10 μM SU5402 (Sigma, D5942) and 10 μM DAPT (Sigma, SML0443) to inhibit VEGF/FGF and NOTCH signalling, respectively, and changed daily for the following 3 days. On day 4, this medium was substituted by N2/B27 medium containing 10 ng/ml bone morphogenetic protein 4 (BMP4, R&D, 314-BP-010) to facilitate the sensory neurogenesis during the next 8 days (Chambers et al., 2012; Reinhardt et al., 2013; Tchieu et al., 2017). On day 5, the smNPC colonies were detached as single cells using Accutase. 0.9×10^6 cells were seeded on Matrigel-coated wells with 2 ml of N2/B27 medium containing 10 ng/ml BMP4. From day 7 to 11 the cells were fed every two days with the same medium. The initial seeding density and BMP4 treatment are critical for a successful differentiation. On day 11, the BMP4 medium was substituted by mature medium containing 500 μM dbcAMP (Sigma, D0627), 10 ng/ml GDNF, BDNF, 25 ng/ml NGF (all from Peprotech) to enhance neuronal differentiation. The medium was changed every 2 days until day 31. Starting from day 32, the cells were cultivated with mature medium lacking dbcAMP. The cells used in most experiments were differentiated for at least 60 days.

Dissociation of day 60 culture: Cells growing in 6-well plate were exposed to 1 ml collagenase IV (Gibco, 200 U/ml, in DMEM) for 15 min, followed by incubation with 1 ml Accutase for additional 60 min, both at 37 °C, mechanically dissociated in 1 ml medium and resultant single cells were seeded on matrigel-coated plates. A high density of seeded cells (0.5 million per cm^2) is critical for survival during subsequent culture.

2.2. Immunofluorescence of cultured cells

Cells were fixed with 3–4% (w/v) paraformaldehyde (PFA) for 20 min, permeabilized and blocked using PBS containing 0.2% (v/v) Triton X-100 and 5% BSA or donkey serum. To stain Piezo1 and Piezo2, PFA fixation was followed by cold methanol incubation as suggested by the manufacturer. Fluorescence images were sequentially acquired using either a Leica TCS SP2 laser scanning inverted confocal microscope (Leica Microsystems, Mannheim, Germany) with the 63.5 × oil-immersion objective or the Observer Z1 microscope (ZEISS) with 63.5 or 100 × oil-immersion objectives.

Data analysis: Confocal images were sequentially captured and stacked with Fiji Image J (NIH). 2D projection images were generated using the tool of maximum intensity projection (Fiji). TIFF images were

imported into Adobe Photoshop CS6 to assemble figures with a resolution of 300 dpi. The numbers of Tuj1, MAP2, Ret, NaV1.7, and TrkB positive neurons and total cells (represented by DAPI staining) were counted using ImageJ with Cell Counter plugin.

To quantify the percentage of co-expression of phosphorylated NF200 and Piezo2, we used two methods. First, we subjectively counted the number of double-positive axons using overlapped images. However, due to the 3D properties of the axon extensions in our culture, some of the axonal boundaries were barely visible, impeding the reorganization of individual axons, thereby influencing counting and quantification. Therefore, we employed an automatic quantification using the ImarisColoc analysis tool (Bitplane), a 3D colocalization method based on volume reconstructions, to compute the co-localization percentages between 2 different channels. In this method, the whole plane of images was defined as region of interest (ROI) for the analysis. Unbiased automatic thresholding of images from each channel was performed using 2D histogram algorithm. The values representing '% of ROI colocalized' obtained with the 'Coloc Volume statistic' were used for quantification. We found in our images that the statistic co-localization percentage reported by the ImarisColoc was about 10% lower than the co-occurrence percentage from subjective counting, suggesting that the ImarisColoc analysis did not over-estimate the co-occurrence percentage.

2.3. Whole cell recordings and mechanical stimulation on cryopreserved SZ-LTMRs

The SZ-LTMRs at 19 or 31 dpd were dissociated with collagenase IV and Accutase. The dissociated cells were frozen using cryopreservation medium CryoStor® CS10 (STEMCELL Technology) previously used to freeze hiPSCs-derived neurons (Rajamani et al., 2018) and transported to the lab where the mechanical stimulation experiments were performed. Prior to the patch-clamp recordings, the dissociated cells were thawed and further cultivated until at least 50 dpd according to the differentiation protocol.

Patch-clamp recordings were performed in the current- and voltage-clamp whole-cell configuration using a Multiclamp 700B amplifier, pCLAMP 10 software and a Digidata 1322A (Molecular Devices, USA). Cells were held at -60 mV and data were sampled at a frequency of 20 KHz and low-passed filtered at 10 KHz. Patch electrodes of 4–7 MΩ were pulled from borosilicate glass capillaries and 70% series resistance compensation was used. The pipettes were filled with an internal solution containing (in mM): 110 KCl, 10 NaCl, 10 HEPES, 1 EGTA, 1 MgCl$_2$ adjusted to pH 7.3 with KOH (280–290 mOsmol/kg^{-1}). Current injection was used to evoke action potentials with pulses varying from -20 pA to 400 nA over 300 ms.

Cells seeded on coverslips were transferred to a recording chamber placed on the stage of a Leica DMI 3000B inverted microscope and perfused with external control solution containing (in mM): 140 NaCl, 3 KCl, 1 CaCl$_2$, 2 MgCl$_2$, 10 glucose and 10 HEPES (pH 7.2; 300 mOsmol/kg^{-1}). Experiments were performed at room temperature ($\sim$24 °C).

Mechanical stimulation of SZ-LTMRs cell bodies was performed by using a heat-closed glass pipette driven by a MM3A-LS piezoelectric micromanipulator (Kleindiek Nanotechnik, Germany). The pipette was positioned on a cell body at a 45–60° angle to the horizontal plane and opposite to the recording pipette and was moved at 540 μm s^{-1}. A series of mechanical steps in 1 μm increments were applied for 250 ms every 10 s.

Mechanically-activated currents were classified by their inactivation time course in rapidly adapting (RA) ($\tau \leq 10$ ms), intermediately (IA) ($10 < \tau < 30$ ms) or slowly adapting currents (SA) ($\tau \geq 30$ ms) as previously described (Hu and Lewin, 2006; Coste et al., 2010). Inactivation time course was adjusted to a mono or double exponential equation using the Clampfit 10 software (Molecular Devices, USA). In the case of fits to a double-exponential, the reported time constant (τ) corresponds to the component with the largest weight.

The rest of Materials and Methods are in the supplementary section.

3. Results

3.1. Generation of human neurons resembling LTMRs

We obtained small molecule-derived neuronal precursor cells (smNPCs) from cord blood-derived iPSC by combining embryoid body (EB) formation and small compounds inhibition (Reinhardt et al., 2013). The Pax6$^+$/Nestin$^+$ smNPCs lacked expression of several peripheral nervous system (PNS)-enriched genes (Fig. S1A). To differentiate the smNPCs into sensory neurons, a published protocol (Reinhardt et al., 2013) was adapted with substantial modifications (details in Methods). The differentiated cells extended processes resembling neurites after 20 days post-differentiation (dpd), and formed spherical cell clusters from 36 dpd (Fig. 1A,B). The clusters were around 600 μm wide, 200 μm thick, with dense projections after 60 dpd. After 80 dpd, the projections assembled into a fiber-like axonal network interconnecting the clusters (Fig. 1B). The cells survived for at least 4 months.

We used, unless otherwise stated, cultures at 60 dpd, exhibiting morphological stability. Comparative transcriptome profiling of the SZ-LTMRs and smNPCs by RNA-seq revealed the induction of genes involved in neuronal development, action potential, ion channel, synaptic transduction and neurotransmission, among others (Fig. S1B). Mitosis-related and DNA repair genes were significantly suppressed (Fig. S1B), consistent with rare BrdU labelling (Fig. S1C). Paired comparison showed differential gene expression between smNPCs and SZ-LTMRs (Fig. 1C). During differentiation, genes enriched in peripheral lineages *SCN9A* and *PRPH* were strongly upregulated, while CNS-specific genes *FOXG1*, *FOXA2* and *SOX21* (Chambers et al., 2012, Ray et al., 2018) remained unaltered (Fig. 1C,F).

The thickness of the clusters impeded light penetration during imaging. Therefore, unless otherwise stated, we dissociated the clusters with collagenase and Accutase to perform immunostainings, patch-clamp and calcium imaging experiments (at least 8 days post-dissociation from 60 dpd neurons). RT-qPCR was done with non-dissociated SZ-LTMRs. Neuronal markers Tuj1, MAP2, and NaV1.7 were highly expressed (84.23 $\pm$ 3.0% and 74.03 $\pm$ 1.8% of SZ-LTMRs expressed Tuj1 or MAP2, respectively; 45.70 $\pm$ 2.3% of Tuj1$^+$ cells expressed NaV1.7) (Fig. 1D,E). We also found some glia cells expressing S100β in the culture (data not shown).

Functionally, approximately 10% of SZ-LTMRs fired spontaneous action potentials (APs) and most of them generated evoked ones (Fig. S1D). The Na$^+$ and K$^+$ channels were functionally active, with the former being tetrodotoxin (TTX)-sensitive (Fig. S1E), mirroring the very low expression of TTX-resistant sodium channels (NaV1.5, NaV1.8 and NaV1.9) (Fig. S1F), ruling out a sympathetic or nociceptive specification of the SZ-LTMRs. Nociceptor-enriched TRP (transient receptor potential) channel agonists failed to evoke Ca^{2+} increase, while KCl did (Fig. S1G). The transcription factor *MASH1*, required for development of sympathetic neurons, was transiently upregulated at 12 dpd (Fig. S1H). However, the sympathetic marker norepinephrine transporter (NET) was not detected and only about 2% of cells expressed tyrosine hydroxylase (TH) at 60 dpd (Fig. S1H,I).

We also addressed the neurotransmitter profiles by HPLC. GABA and glutamate, characteristic of somatosensory neurons (Du et al., 2017), were detected in large quantities in the supernatant and cell lysates of non-dissociated SZ-LTMRs at 60 dpd (Fig. 1G). The concentrations of acetylcholine (Ach), adrenaline and serotonin were very low, while dopamine was undetectable, ruling out an autonomic phenotype (Matthes and Bader, 2018). The high abundance of glutamate synthesis was consistent with the induction of vesicular glutamate transporters *VGLUT2* and *VGLUT3*, but not CNS-enriched *VGLUT1* (Jarvie and Hentges, 2012) (Fig. S2A). RNA-seq also revealed the upregulation of GABA related genes *GAD1*, *GAD2*, *SLC32A1* and the fate determinants of GABAergic neurons *DLX1*, *2*, and *5* (Yang et al., 2017) (Fig. S2B). Furthermore, a significant proportion of dissociated SZ-LTMRs, but not HEK cells, expressed both glutamate and GABA (Fig. S2C,D), suggesting the co-synthesis of both
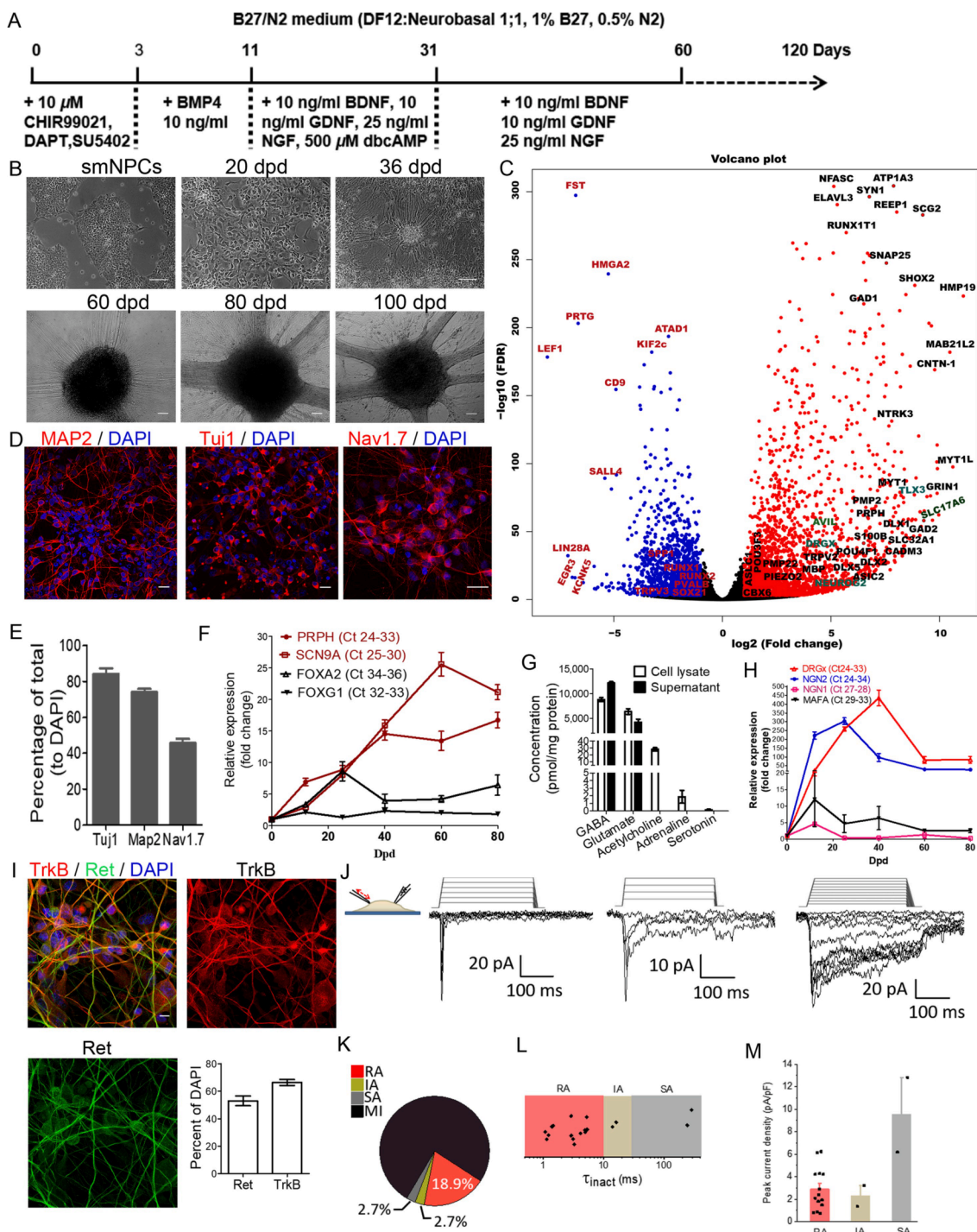
Fig. 1. Differentiation of smNPCs into neurons with characteristics of LTMRs. (A) Schematic illustration of the differentiation protocol, including the different treatments performed. (B) Morphological changes during the differentiation process. N > 30 independent differentiations. Bars, 100 μm. (C) Volcano plot showing differentially expressed genes in the non-dissociated SZ-LTMRs at 60 dpd versus smNPCs. Upregulated (red) and downregulated (blue) genes are shown. Thresholds for false discovery rate (FDR) and Log 2-fold change were 0.001 and 1, respectively. (D) Projection of confocal Z-stacks showing expression of MAP2, Tuj1 and NaV1.7 in SZ-LTMRs at 8 days post-dissociation from 60 dpd cultures. Bars, 20 μm. (E) Graph showing percentages of neurons positive for Tuj1, MAP2 and NaV1.7 (N = 434, 467 and 389 cells, respectively). (F) Fold changes (versus smNPCs) of *PRPH, SCN9A, FOX2A and FOXG1* mRNA (normalized to *GAPDH*) during differentiation, quantified by RT-qPCR. (N = 4). (G) Concentration of selected neurotransmitters in cell lysates and supernatants of non-dissociated SZ-LTMRs at 60 dpd. N = 12 technical replicates. (H) Fold changes (versus smNPCs) of *DRGX, NGN2, NGN1, and MAFA* mRNA (normalized to *GAPDH*) during differentiation, quantified by RT-qPCR. N = 3–4. (I) Projection of confocal Z-stacks showing TrkB and Ret in 8 days post-dissociated SZ-LTMRs from 60 dpd cultures. Bars, 10 μm. Graph showing percentages of positive neurons. N = 465 (TrkB) and 401 (Ret) cells. (J) Representative traces of the three subtypes of mechanically activated currents, rapidly adapting (RA), intermediately adapting (IA) and slowly adapting (SA, from left to right) recorded from dissociated SZ-LTMRs at around 50 dpd. The average mechanical thresholds of RA, IA and SA are 10.4 ± 0.7, 10.5 ± 0.5 and 5 ± 2 μm, respectively. (K) Pie plot showing the distribution of mechano-sensitive (18/74) and mechano-insensitive (MI) SZ-LTMRs (56/74); the proportion of the different types of mechanically-activated (MA) currents is displayed with respect to the total number of MA recorded neurons (n = 74). (L) Average inactivation kinetics (τ) of different types of MA currents from all the cells. (M) Average values of peak current density from cells producing different types of MA currentsEach dot represents one cell. Values are presented as mean ± s.e.m.

neurotransmitters. Additionally, the glutamatergic marker VGLUT2 and the GABAergic marker GAD67 were expressed in the same neurons (Fig. S2E). These results collectively suggested that the SZ-LTMRs might be glutamatergic and GABAergic, resembling a subset of mDRG neurons *in vivo* (Du et al., 2017). The SZ-LTMRs synthesized trace amount of Ach (Fig. 1G), consistent with the low expression of choline acetyltransferase (*CHAT*) (Fig. S2F), the enzyme responsible for Ach synthesis. It is worth noting that rat DRG neurons also synthesize Ach (Bellier and Kimura, 2007). The same smNPCs can be primed to derive motor neurons (Naujock et al., 2014), which require *ISL1* for generation and survival, and express *CHAT* for Ach synthesis. Lack of ISL1 expression (Fig. S2F) rules out the possibility that SZ-LTMRs resemble motor neurons, indicating that the smNCPs can be differentiated into different neuronal subtypes. Overall, the expression and neurotransmitter profile of the SZ-LTMRs after 60 dpd suggested a PNS specification, but they were neither sympathetic nor nociceptive.

We next examined the markers expressed in sensory neurons. About 81 genes were identified as DRG-enriched when comparing the transcriptome of human DRG with those of 13 different tissues (Ray et al., 2018). The genes with highest DRG enrichment scores (>100 transcripts per million), such as *STMN2*, *UCHL*, *GNG3*, *SNCG*, or the ones specific to DRG, such as *AVIL* and *HTR3A*, were significantly upregulated in the SZ-LTMRs (Fig. S2G). Several transcription factors regulating the hDRG transcriptomic landscape, (Zurborg et al., 2011, Ray et al., 2018), including *SHOX2*, *SCRT2*, *POU4F1*, *POU4F2*, *TLX3* and *DRGx*, were *de novo* induced (Fig. S2G). Transcription of *SCN10A*, *SCN11A*, and *RUNX1* specific to small-sized nociceptive DRG neurons, was minimal in the SZ-LTMRs, although *PRDM12* was slightly, but not significantly, induced (Fig. S2G). In contrast, several genes enriched in large-sized DRG neurons, *NTRK2*, *NTRK3*, *CNTN1*, (Miura et al., 2015) *GABRB3*, (Orefice et al., 2016) and *TRPV2*, (Usoskin et al., 2015) were significantly upregulated (Fig. S2G). The proprioceptor markers *PVALB* and *SPP1*, (Usoskin et al., 2015) and the fate determinant *RUNX3* (Levanon et al., 2002) were not increased (Fig. S2G).

We then focused on genes typically expressed in LTMRs. RT-qPCR analysis showed robust induction of *NGN2*, one crucial fate determinant of LTMRs expressing TrkB and/or TrkC, (Bourane et al., 2009) but not of *NGN1*, required for development of TrkA^{+} DRG neurons (Lallemend and Ernfors, 2012) (Fig. 1H). *MAF* (encoding c-Maf), controlling LTMRs development, (Wende et al., 2012) was significantly upregulated (Fig. S2G). However, we observed a weak and transient induction of *MAFA*, a gene expressed in the early Ret[+] LTMR subpopulation (Lecoin et al., 2010) (Fig. 1H). *TRKB/C* but not *TRKA* were transcriptionally induced (Fig. S2H). 66.33 ± 2.2% and 52.88 ± 3.5% of dissociated SZ-LTMRs were TrkB[+] and Ret[+], respectively (Fig. 1I). The high expression of TrkB was also supported by the robust induction of *Shox2* (Fig. S2G), a transcription factor driving the generation of TrkB[+] LTMRs (Abdo et al., 2011). We visualized TrkB in non-dissociated clusters by light-sheet fluorescence microscopy (Fig. S2I). NF200, a protein enriched in human DRG neurons, was present in 71.69 ± 10.9% of MAP2^{+} dissociated SZ-LTMRs (Fig. S2J). *CALB* and *FAM19A1*, two novel LTMRs markers, (Usoskin et al., 2015) were dramatically induced following differentiation (Fig. S2H). Lack of TH (Fig. S1I) and RUNX1 (Fig. S2G) rules out the possibility that SZ-LTMRs resemble C-LTMRs (Li et al., 2011).

The overall profile of gene expression prompted us to assess the mechanosensitivity of SZ-LTMRs, a hallmark of LTMRs. We applied indentation to the cell surface using an electrical-driven glass pipette and recorded the responses using the voltage-clamp configuration at a holding potential of −60 mV. We observed that, despite one freeze–thaw cycle (see Methods), 24.3% of the cells still displayed mechanosensitivity by generating RA, IA or SA (Fig. 1J,K), based on their inactivation time course. All the MA currents showed graded increases in amplitude in response to progressively larger indentation values (Fig. 1J), and were mainly RA (Fig. 1K). Average inactivation kinetics (τ) of each type of currents were 3.1 ± 0.4, 15.1 ± 1.1 and 264.4 ± 21.1 ms for RA, IA, SA (Fig. 1L), respectively, similar to MA currents described in mouse

mechanosensitive neurons (Coste et al., 2010, Hu and Lewin, 2006). The average value of peak current density was significantly higher in SA neurons (9.5 ± 3.3 pA/pF), compared to RA (2.9 ± 0.5 pA/pF) and IA (2.3 ± 0.9 pA/pF) neurons (Fig. 1M), recapitulating that of mouse sensory neurons observed in our previous study (Fernández-Trillo et al., 2020). Overall, these results (low mechanical thresholds versus high current densities) suggest that at least a subset of SZ-LTMRs is mechanosensitive.

3.2. Piezo2 concentrates within enlarged axonal termini

Since Piezo2 is the main established mechanotransducer in LTMRs, we used a previously validated antibody (Narayanan et al., 2016; Goto et al., 2020; Lu et al., 2020; Alcaino et al., 2017), to address its expression in the SZ-LTMRs. In non-dissociated cultures, strong signals from Piezo2 and phosphorylated NF200 (pNF200), the axonal form of NF200, were detected in round structures that had diameters ranging 2–10 μm, and were DAPI negative (Fig. 2A). Quantification showed that Piezo2^{+} structures were 34.7 ± 9.3% of total cells, and 61.2% of Piezo2^{+} structures co-expressed pNF200 (Fig. 2A). We hypothesized that during microscopic imaging, the thickness of the compact clusters at 60 dpd impeded light traveling to capture relatively weak signal from Piezo2 and pNF200. We thus dissociated the clusters into single cells. In 8 days post-dissociated neurons from 60 dpd culture, pNF200 and Piezo2 were both detected along axons and concentrated at enlarged axonal termini (Fig. 2B). Coincidently, a recent paper (Johnson et al., 2021) reported that a custom-made polyclonal antibody for spider Piezo protein also gave rise to stronger signal in the nerves than in somata in the VS-3 slit sensillum, a small mechanoreceptory organ sensing physical deformation or strain. Further quantification showed Piezo2 axons accounted for 44.5 ± 6.6% pNF2002[+] axons (Fig. 2C). We also detected relatively weak and strong Piezo2 signals in axons and termini, respectively, from non-dissociated SZ-LTMRs at 36–40 dpd, when cells did not form similar large clusters with those in 60 dpd culture that impeded light traveling (Fig. 1B). Moreover, the staining signal was moderately lower in SZ-LTMRs stably expressing Piezo2 shRNA than shRNA control, indicating the specificity of the antibody (Fig. S3A,B). Thus, some axon termini from non-dissociated and dissociated SZ-LTMRs enlarged to form bulbous structures, which were morphologically distinct from growth cones, the flat, sheet-like protrusions of growing axons (Fig. S3C and (Specht et al., 1981)). Notably, *in vivo*, some nerve endings of LTMRs are also enlarged, forming bulb-like expansions (García-Mesa et al., 2017; Nolano et al., 2003; Nolano et al., 2008), containing Piezo2 (Woo et al., 2014; García-Mesa et al., 2017).

We next characterized the bulbous structures using dissociated SZ-LTMRs. Some Piezo2^{+} or pNF200[+] structures contained Ret, NaV1.7, and Peripherin and lacked Tuj1 (Fig. S3D-G). The Piezo2 structures in the SZ-LTMRs were TH negative (Fig. S3H), in contrast to RNA-seq data suggesting that *PIEZO2* is enriched in the TH[+] mDRG subset (Usoskin et al., 2015). Single focal plane image showed that α-tubulin was not concentrated in the structure (Fig. S3I), while projection of Z-stack images showed that tubulin bundles surrounded the enlarged termini (Fig. S3J). These data suggested that the structures have a specialized molecular composition.

We also asked whether the Piezo2^{+} structures, especially the ones in dissociated SZ-LTMRs, were unhealthy termini due to the dissociation process that may lead to enlarged termini termed retraction bulbs, which, however, mainly appear in damaged axons from the CNS but not PNS (Sherriff et al., 1994). To rule out this possibility, we monitored the morphology of the dissociated cells by phase contrast microscopy. Neurite number and length increased over time and cells survived longer than 13 days post-dissociation (Fig. S3K). The cells progressively formed small clusters, mimicking the behavior of primary mDRG culture in dishes (Fig. 3F). Neurofilament L (NFL) staining confirmed the gradual increase of axonal densities (Fig. S3L). Moreover, the mRNA of several genes involved in stress response (*ERG1*), axon destruction (*DLK1*), regeneration (*ATF3*), and maintenance (*NMAT2*), was similar between the non-
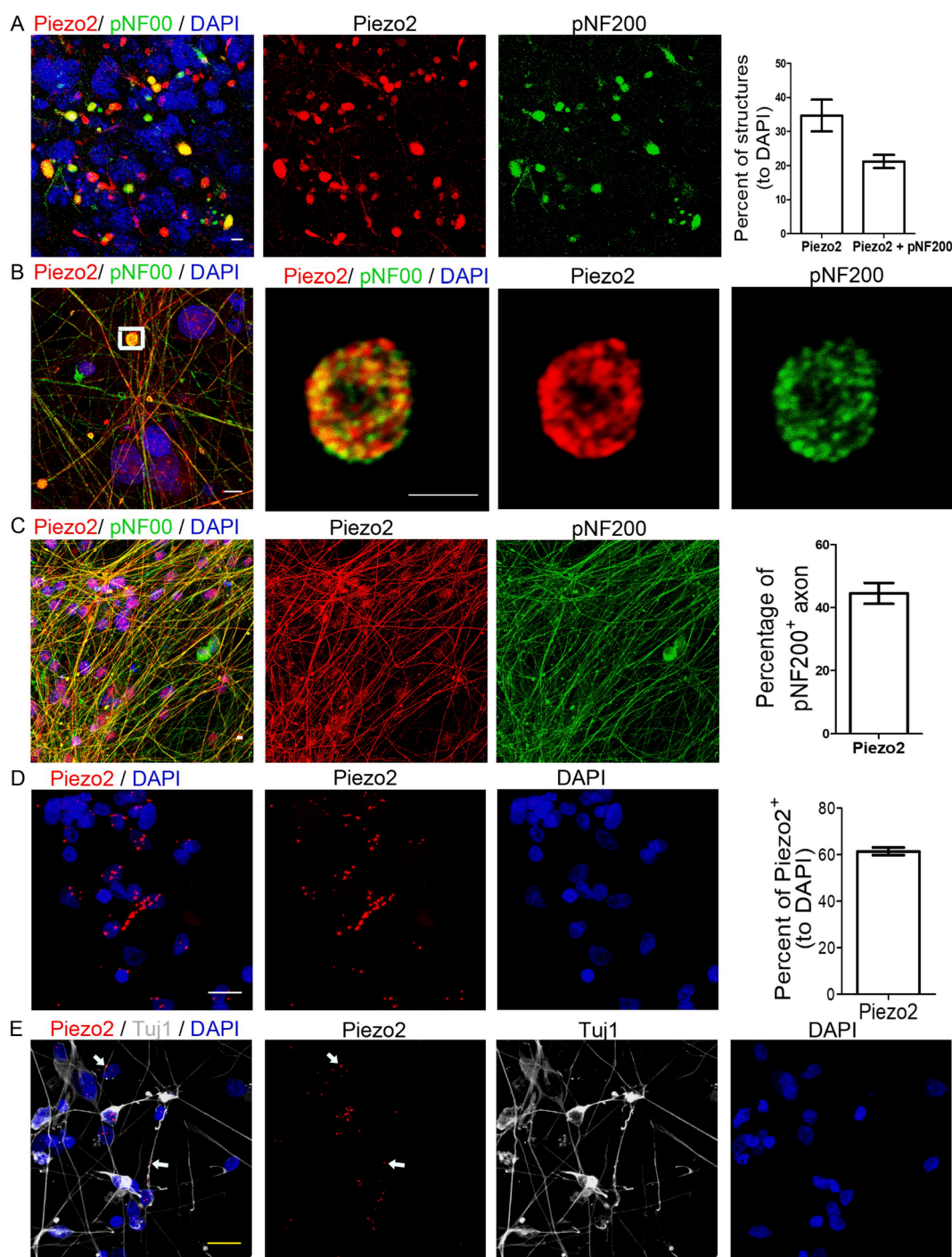
Fig. 2. Enrichment of Piezo2 within enlarged axon termini of the SZ-LTMRs. (A-C) Immunofluorescence showing Piezo2 and pNF200 in non-dissociated (A) and dissociated (B,C) SZ-LTMRs. Graph in (A) shows the percentage of Piezo2 and Piezo2/NF200 double positive structures (right, N = 4). Boxed region in (B) is enlarged in the three panels on the right (N > 7). Graph in (C) shows the percentage of Piezo2$^+$ axons (normalized to pNF200$^+$, N = 4). Bars, 5 μm. (D, E) Detection of Piezo2 mRNA in dissociated SZ-LTMRs by RNAscope fluorescent multiplex assay alone (D) or in combination with Tuj1 staining (E). The graph in (D) is from 806 cells from 3 independent experiments. Arrow in E shows axonal distribution of Piezo2 mRNA. N = 2. Bars, 20 μm. Images except for the enlarged boxed region in (B) are projections of confocal Z-stacks. Dissociated SZ-LTMRs refer to cells that are 8 days post-dissociation from 60 dpd cultures. Values are presented as mean ± s.e.m.

dissociated and 3 days post-dissociated SZ-LTMRs (Fig. S3M). These observations suggested that typical axon damage response was not largely induced after 3 days post-dissociation. Based on this and the observed surrounding of α-Tubulin bundles (Fig. S3J) that is substantially devoid in retraction balls (Ertürk et al., 2007), and lack of amyloid precursor protein (Fig. S3N) that accumulates in damaged axons (Coleman, 2005), we thus concluded that Piezo2$^+$ structures in dissociated SZ-LTMRs represent axonal termini of healthy neurons, echoing with the functionality of the

dissociated SZ-LTMRs in generation of action potentials, Na and K currents, and response to KCl, etc.

We further proved the expression of Piezo2 in the SZ-LTMRs by in situ hybridization using RNAscope (Fig. 2D,E). We detected Piezo2 mRNA in 61.4 ± 1.6% of SZ-LTMRs, in both cell bodies and axons, even when treatment for Tuj1 immunofluorescence staining subsequent to ISH weakened the mRNA signal (Figs. 2D, E, 4B). Axonal distribution of Piezo2 mRNA suggests that an efficient protein synthesis is required for axon
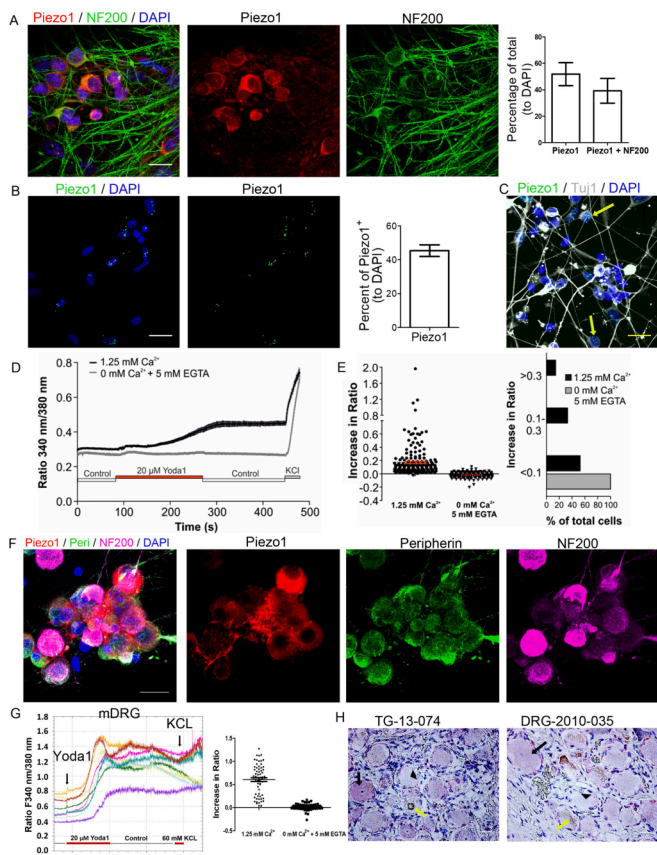
Fig. 3. Presence of Piezo1 in the SZ-LTMRs and human sensory ganglia. (A) Co-expression of Piezo1 and NF200 in dissociated SZ-LTMRs. Graph shows percentage of Piezo1$^+$ and Piezo1$^+$ NF200$^+$ cells (N = 4–5). Bar, 20 μm. (B,C) Detection of Piezo1 mRNA alone (B) and together with β-Tubulin-III protein (C, indicated by arrows) in dissociated SZ-LTMRs. Graph in (B) shows percentage of Piezo1$^+$ cells (N = 964 cells). Bars, 20 μm. (D) Average F340/380 ratio of dissociated SZ-LTMRs challenged with 20 μM Yoda1 in standard Ca^{2+}-containing solution (black, n = 188) or in Ca^{2+}-free solution (grey, n = 249). 60 mM KCl was applied at the end of the experiments to verify a neuronal phenotype of the recorded cells. (E) Scatter plot (left) and percentages of Yoda1 responsive cells (right) showing the response or lack of response of individual SZ-LTMRs represented as F340/380 nm ratios following application of Yoda-1 in standard Ca^{2+}-containing solution or without Ca^{2+}. Each dot represents one cell. (F) Presence of Piezo1, peripherin and NF200 in cultured mDRG neurons. Some of the single Z-sections are shown in Fig. S4O. N = 7. Bar, 20 μm. (G) Representative traces (left) showing the time-lapse recording of Yoda1-induced Ca^{2+} flux in Yoda1 (20 μM) challenged mouse primary DRG neurons. Graph (right) showing Yoda1 induced increase of F340/380 ratios from individual cells. N = 63 (1.25 mM Ca^{2+}) and 101 (0 mM Ca^{2+} 5 mM EGTA) cells, respectively. (H) Detection of Piezo1 mRNA in hTG and hDRG tissues by RNAscope. Black arrows and arrowheads indicate neurons with and without pink puncta, respectively, indicating Piezo1 mRNA. Yellow arrows point to lipofuscin granules. Stronger intensity was detected at the periphery of neurons and in surrounding non-neuronal cells. Bars, 25 μm. All confocal images are projections of Z-stacks. Dissociated SZ-LTMRs refer to cells at 8 days post-dissociation from 60 dpd cultures. Values are presented as mean ± s.e.m.

biology, echoing with the high Piezo2 protein levels detected in axons (Fig. 2C). We did not detect Piezo2 protein in the majority of smNPCs, except in few spontaneously differentiated cells expressing NF200 (Fig. S3O). However, *PIEZO2* mRNA levels were significantly upregulated upon neural differentiation, albeit at moderate levels (Fig. S3P).

Lastly, we found that the antibody recognizing residues 1600–1650 stained soma localized Piezo2 in mouse DRG neurons (Fig. S4N), but not in SZ-LTMRs (Fig. 2B), Piezo2 gene has >18 variants in sensory neurons (Szczot et al., 2017). Lack of Piezo2 in the soma of SZ-LTMRs could be

due to a possible difference in Piezo2 splicing between human and mouse (Szczot et al., 2017), resulting in a Piezo2 variant(s) located in the soma of the SZ-LTMRs that is not detected by this antibody. Alternatively, the different staining patterns observed between SZ-LTMRs and mDRG could also be due to differences in the cell culture conditions and/or to antibody specificity. We used the other Piezo2 antibody, recognizing residues 146–212, to stain non-dissociated, and 8 days post-dissociation SZ-LTMRs (Fig. S3Q, left and right, respectively). Both Piezo2 antibodies stained the Piezo2 structures in non-dissociated neurons. However, we detected Piezo2 in the cell bodies and enlarged bulbous structures of SZ-LTMRs with the second Piezo2 antibody (recognizing residues 146–212; Fig. S3Q, right). We also confirmed the specificity of this antibody in 1 day post-dissociation SZ-LTMRs expressing shPiezo2 (Fig. S3R).

Overall, our results suggest that the SZ-LTMRs express Piezo2 at the axon termini, axons and cell bodies in both dissociated and non-dissociated neurons. Hence, we generated human LTMRs that have specialized axon termini morphologically resembling bulbous nerve endings

3.3. Piezo1 is expressed in SZ-LTMRs and human sensory ganglia

We next addressed whether the SZ-LTMRs expressed Piezo1 using a previously validated anti-Piezo1 antibody (Gudipaty et al., 2017, Jetta et al., 2019, Mazzuoli-Weber et al., 2019, Silver et al., 2020, Yao et al., 2020). We further validated this antibody using ARPE-19 cells, a human epithelial cell line expressing high level of *PIEZO1*, but not *PIEZO2* mRNA (Fig. S4A). Two commercial siRNAs targeting *PIEZO1* (siRNA1724 and siRNA1725), but not an siRNA control, reduced Piezo1 signal at the cell surface (Fig. S4B,C), confirming the specificity of the antibody, as before (Gudipaty et al., 2017), although plausible non-specific signal was found in the nucleus of knockdown cells (Fig. S4B). We detected Piezo1 within cell bodies, but not axons, of 51.84 ± 8.71% of dissociated cells, co-expressed with NF200 in 39.23 ± 9.44% of total cells (Fig. 3A). Incubation with the immunizing antigen peptide depleted Piezo1 staining in SZ-LTMRs (Fig. S4D). RNAscope showed that 45.40 ± 3.465% of SZ-LTMRs transcribed Piezo1 mRNA (Fig. 3B). These cells expressed Tuj1 (Fig. 3C). The RNAscope probe was Piezo1 specific since siRNA1724 decreased the signal in ARPE19 cells while the non-targeting siRNA did not (Fig. S4E). Furthermore, knockdown of Piezo1 by lenti-shRNAs in SZ-LTMRs decreased the immunostaining signal (Fig. S4F,G), further supporting the specificity of the antibody staining.

To further confirm Piezo1 expression, we measured Ca^{2+} responses induced by Yoda1, a Piezo1-specific irreversible agonist (Syeda et al., 2015). Yoda1 induced low but significant Ca^{2+} influxes in 8–12 days post-dissociated SZ-LTMRs, with an average F340/380 ratio of +0.17 ± 0.02 and −0.01 ± 0.002 in the presence and absence of extracellular calcium, respectively (Fig. 3D,E). The large majority of cells were responsive to 60 mM KCl (Fig. 3D), confirming their neuronal fate. Representative traces during the time-lapse recording of SZ-LTMRs are shown in Fig. S4H, consistent with previous studies showing that Yoda1-induced calcium influx is slow, without decay, and poorly reversible in non-neuronal cells (Wang et al., 2018; Syeda et al., 2015), and neuronal cell line N2A (Zhang et al., 2017) wherein Piezo1 was discovered as a mechanotransducer (Coste et al., 2010). Based on the Yoda1 responses, SZ-LTMRs were classified as high (F340/F380 ratio higher than 0.3, 14.3% of the total cells), low (F340/F380 ratio 0.1–0.3, 38.8% of the total cells), and negative (F340/F380 ratio lower than 0.1, 46.9% of the total cells) (Fig. 3E). Furthermore, the Yoda1 induced Ca influx was largely suppressed in SZ-LTMRs expressing shPiezo1 (Fig. S4I). Collectively, these results indicated that over 50% of SZ-LTMRs expressed functional Piezo1 at low level recapitulating *in vivo* situation.

We next asked whether Piezo1 expression was induced following differentiation. *PIEZO1* mRNA remained low during the differentiation process (RT-qPCR, Fig. S4J). Five different regions covering representative parts of full-length *PIEZO1* mRNA were also weakly detected in the SZ-LTMRs by conventional RT-PCR (Fig. S4K). However, Piezo1 protein

was not detected in most smNPCs by the antibody used except in few cells spontaneously expressing NF200 (Fig. S4L), indicating that *PIEZO1* expression could be post-transcriptionally induced in the SZ-LTMRs (further discussed below). Furthermore, the inconsistence between *PIEZO1* mRNA and protein levels is also described elsewhere (https://www.proteinatlas.org/ENSG00000103335-PIEZO1/tissue). This led us to address *PIEZO1* protein expression in mDRG neurons, where the channel is functionally active (Song et al., 2019), despite low mRNA levels (Coste et al., 2010, Ranade et al., 2014). Projections of Z-stack confocal images showed that a substantial portion of primary cultured mDRG neurons expressed Piezo1 (Fig. 3F). Three of the single Z-sections showed Piezo1 signal at the cell surface, cytoplasm, and nuclear membrane (Fig. S4M). The nuclear envelope signal suggested a possible non-specific staining, although nuclear immunoreactivity for the same antibody was reported to be specific to Piezo1 in epithelial cells (Jetta et al., 2019). Similar to the pattern observed in SZ-LTMRs, Piezo1 in mDRG neurons was mainly compartmentalized within the soma (Fig. 3F), while Piezo2 was found in both axons and soma (Fig. S4N). Functionally, around 79% of cultured mDRG neurons responded to Yoda1, with an average F340/380 ratio of 0.56 ± 0.04 that was higher than 0.17 ± 0.01 in SZ-LTMRs (Fig. 3E,G). However, Yoda1 has a lower EC50 for mouse (17.1 μM) than for human Piezo1 (26.6 μM) (Syeda et al., 2015).

We also addressed Piezo1 expression in human sensory ganglia. *PIEZO1* mRNA was weakly detected by RNAscope in some neurons in one hTG and hDRG (Fig. 3H), similar with the low mRNA level in SZ-LTMRs (Fig. 3B, S4L, M). We observed higher and more uniform *PIEZO1* mRNA in non-neuronal cells than in neurons (Fig. 3H), although Piezo1 was initially identified as a neuron-specific gene in normal brain tissue (Satoh et al., 2006). Our data collectively suggest that Piezo1 is expressed in sensory neurons, consistent with a recent report (Roh et al., 2020).

Piezo1 protein synthesis is induced from low abundance mRNA in SZ-LTMRs (Fig. S4J,K,) and mDRG (Ranade et al., 2014). Several mechanisms, including epigenetic regulation and non-coding RNAs (ncRNAs), influence mRNA translation. Human genomic annotation data showed 3 antisense ncRNAs predicted to target *PIEZO1* (Fig. S4O). Two of them (LOC339059 and LOC100289580) were upregulated following differentiation. The untranslated regions (UTRs) of human *PIEZO1* mRNA have high GC contents indicative of structural stability. Both UTRs were predicted by RNAfold software to form secondary structures with multiple loops. RNA looping at the 5′-UTR generally enhances translation efficiency by facilitating 40S ribosome scanning (Paek et al., 2015). The IRESPred tool predicted that human *PIEZO1* 3′-UTR contains a potential internal ribosomal entry site element, known to increase the translation of upstream mRNA (Paek et al., 2015). Additionally, *PIEZO1* mRNA has a Kozak-like sequence (CCAGCC**AUG**G), optimizing translation. Finally, it is possible that the half-life of *PIEZO1* mRNA is much lower than that of the protein. Overall, these factors may determine Piezo1 protein synthesis in DRG neurons expressing low mRNAs. Thus, *PIEZO1* expression in the SZ-LTMRs could be induced by post-transcriptional regulatory mechanisms, known to control gene expression during neuronal differentiation *in vitro* and *in vivo* (Baser et al., 2019).

Overall, the SZ-LTMRs expressed low level of Piezo1 at mRNA levels, mimicking what is found in human tissues. Despite this, the SZ-LTMRs could efficiently synthesize functional Piezo1 protein from low mRNA level. Thus, we generated the first stem cell-derived human sensory model to study Piezo1.

3.4. A subset of SZ-LTMRs co-express Piezo1 and Piezo2

Given that SZ-LTMRs expressed Piezo1 and Piezo2, and a small proportion of mDRG neurons co-express Piezo1/2 mRNAs ex vivo (Wang et al., 2019), we then asked whether the SZ-LTMRs co-express Piezo1/2 by RNAscope. As shown in Fig. 4A, $31.4 \pm 1.3\%$ of SZ-LTMRs co-
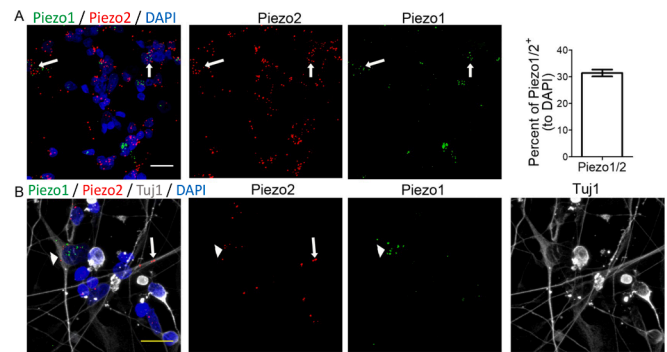

Fig. 4. Co-expression of Piezo1 and Piezo2 in SZ-LTMRs. (A,B) Projections of confocal Z-stacks showing Piezo1 and Piezo2 mRNA alone (A) or together with β-Tubulin-III protein (B) in dissociated SZ-LTMRs. The graph in (A) shows the percentage of Piezo1⁺/Piezo2⁺ cells from 3 independent experiments (N = 669 cells). The white arrow in (A) points to cells of co-expression of Piezo1 and Pieo2. The arrowhead and arrow point to Piezo1/2 double positive neurons and axonal distribution of Piezo2 mRNA, respectively. Bar, 25 μm. Mean ± s.e.m.

expressed Piezo1/2 mRNAs. RNaseA treatment resulted in lack of detected transcripts (Fig. S5). Combination of RNAscope and Tuj1 staining showed co-expression of Piezo1/2 in SZ-LTMRs, with Piezo2 mRNA distribution in some axons (Fig. 4B).

4. Discussion

We established a differentiation protocol to generate neurons resembling human LTMRs from smNPCs that were derived from iPSCs. As shown in the original study (Reinhardt et al., 2013), the cellular identity of smNPCs mimics that of neural plate border cells. The smNPCs express PAX6 and SOX9, markers of neuroectoderm and neural crest cells, respectively. Those cells are multipotent to differentiate into both PNS and CNS lineages. For instance, the smNPCs used in this study were primed by retinoic acid for generation of motor neurons (Naujock et al., 2014). In our protocol, we primed the smNPCs into PNS lineage by sequential activation of WNT and BMP4 signaling. The smNPCs can be easily propagated, and their multipotency is retained over multiple passages. One advantage of the protocol is the avoidance of iPSCs cultivation, which may cause variation among batches and passages. This differentiation protocol is highly robust as shown by the morphological consistence over 30 differentiations performed so far. The presence of NGF did not induce presence of nociceptors in our differentiated culture, as observed previously (Schrenk-Siemens et al., 2015).

We demonstrated the LTMR phenotype by showing the expression of specific markers including *NGN2, SHOX2* and *MAF* for fate specification of TrkB⁺Ret⁺ LTMRs subtype, the co-synthesis of GABA and glutamate for neurotransmission, and the expression of Piezo1 and/or Piezo2 for mechanotransduction. Human LTMRs expressing Piezo2 and responding to mechanical indentation were previously derived from iPSCs (Schrenk-Siemens et al., 2015, Nickolls et al., 2020, Saito-Diaz et al., 2021). In these LTMRs producing RA currents only, the sole mechanotransducer was Piezo2, and its subcellular location was not addressed. It would be also interesting to check the functional expression of Piezo1 in the human LTMRs reported previously (Schrenk-Siemens et al., 2015, Nickolls et al., 2020, Saito-Diaz et al., 2021).

One interesting finding of our study is the generation of enlarged Piezo2⁺ end structures that have a morphology of bulbous nerve endings, providing the first human model to investigate the specialized structures in a context of neuronal integrity, when compared to mouse skin-nerve preparations, an *ex vivo* model lacking neuronal somata. Isolation of Piezo2⁺ structures by synaptosome preparation strategy

used in our previous study (Zhu et al., 2015)₂ will help characterizing their molecular composition. Furthermore, the enlarged termini provide an *in vitro* model for recording mechanosensitivity of axonal endings.

We showed expression of Piezo1 in the SZ-LTMRs and in human sensory neurons by antibody staining and RNAscope. Whether Piezo1 functions as a mechanotransducer in SZ-LTMRs remains to be confirmed. However, a recent study reported that cultured mouse and human DRG neurons express functional Piezo1 (Roh et al., 2020). In that study, 10 μM Yoda1 induced transient, and reversible calcium signals in the majority of DRG neurons, differing from the slow and irreversible patterns observed in our SZ-LTMRs and other studies (Zhang et al., 2017; Wang et al., 2018; Syeda et al., 2015). This discrepancy could be due to the concentrations of Yoda1 used. Since Yoda1 has very high EC50 for human Piezo1 (Syeda et al., 2015), we speculate that lower concentration of 10 μM could induce reversible calcium signals, as shown in the study (Roh et al., 2020). Moreover, the SZ-LTMRs express low level of functional Piezo1 and slowed response to Yoda1 compared to ARPE-1 cells and similar to those of sensory neurons *in vivo*.

One controversial finding of our report is the subcellular location of Piezo1. In the SZ-LTMRs and cultured mDRG neurons, it is mainly restricted to the cell bodies. This is inconsistent with a recent study showing that Piezo1 inhibits axonal regeneration of peripheral sensory neurons during injury (Song et al., 2019), pointing to a potential location in the axons. However, nerve injury can trigger transportation of soma components required for mechanoelectrical transduction to the injured afferents (Koschorke et al., 1994), resulting in ectopic expression of mechanotransducers at the injury site, where an enhanced mechanical sensitivity is developed (Koschorke et al., 1994). It is unknown whether this axonal location of Piezo1, if it exists, is due to an injury-dependent in situ upregulation, or a redistribution of soma-located Piezo1.

We observed co-expression of Piezo1 and Piezo2 mRNAs in some SZ-LTMRs. Since Piezo2 is the well-established mechanotransducer, we suggest that at least the SZ-LTMRs co-expressing Piezo1 and Piezo2 have characteristics of LTMRs. This, in turn, indicates the presence of Piezo1 in this subtype. It was previously reported that knockdown of Piezo1 in mDRG neurons slightly (but not significantly) decrease IA currents (Ranade et al., 2014), which requires simultaneously activated RA and SA channels (Rugiero et al., 2010). Moreover, broad expression of exogenous Piezo1 in mouse DRG *in vivo* selectively enhances IA current production (Zhang et al., 2019). We observed that small proportion of SZ-LTMRs generated intermediately adapting (IA) currents (Fig. 1J). Whether Piezo1 and Piezo2 generate SA and RA currents, respectively, and together produce IA currents, warrants future study using the SZ-LTMRs as suitable model.

Overall, we have generated a robust differentiation method to obtain human LTMRs that contain bulbous nerve endings containing Piezo2. About half of the SZ-LTMRs express Piezo1, and some co-express both channels, providing the first *in vitro* model to study the role of both channels in human LTMRs. We believe that these neurons will serve as a model to study human mechanotransduction.

Funding

CRediT authorship contribution statement

Shuyong Zhu: Conceptualization, Data curation, Formal analysis, Investigation, Methodology, Validation, Visualization, Writing - original draft, Writing - review & editing. **Nancy Stanslowsky:** Methodology. **Jorge Fernández-Trillo:** Formal analysis, Investigation, Methodology. **Tamrat M. Mamo:** Formal analysis, Methodology. **Pengfei Yu:** Methodology. **Norman Kalmbach:** Formal analysis, Methodology. **Birgit Ritter:** Methodology. **Reto Eggenschwiler:** Formal analysis, Investigation, Methodology, Validation, Visualization, Writing - review & editing. **Werner J.D. Ouwendijk:** Methodology. **David Mzinza:** Formal analysis, Methodology. **Likai Tan:** Formal analysis. **Andreas Leffler:** Formal analysis, Investigation, Methodology, Resources. **Michael Spohn:** Formal analysis. **Richard J.P. Brown:** Formal analysis, Writing - review & editing. **Kai A. Kropp:** Methodology, Writing - review & editing. **Volkhard Kaever:** Formal analysis, Methodology. **Teng-Cheong Ha:** Formal analysis, Methodology. **Pratibha Narayanan:** Formal analysis, Methodology. **Adam Grundhoff:** Formal analysis. **Reinhold Förster:** Resources, Writing - review & editing. **Axel Schambach:** Resources, Writing - review & editing. **Georges M.G.M. Verjans:** Formal analysis, Resources. **Manuela Schmidt:** Formal analysis. **Andreas Kispert:** Formal analysis, Resources. **Tobias Cantz:** Formal analysis, Resources, Investigation, Writing - review & editing. **Ana Gomis:** Formal analysis, Investigation, Methodology, Resources, Writing - review & editing. **Florian Wegner:** Formal analysis, Investigation, Methodology, Resources, Writing - review & editing. **Abel Viejo-Borbolla:** Conceptualization, Data curation, Formal analysis, Investigation, Project administration, Resources, Supervision, Validation, Visualization, Writing - original draft.

Declaration of Competing Interest

The authors declare that they have no known competing financial interests or personal relationships that could have appeared to influence the work reported in this paper.

Acknowledgements

Data availability

The raw and processed RNA-seq data has been submitted to Gene Expression Omnibus (GEO) as a GEO project and will be openly available.

Appendix A. Supplementary data

Supplementary data to this article can be found online at https://doi.org/10.1016/j.scr.2021.102535.

References

Abdo, H., Li, L., Lallemend, F., Bachy, I., Xu, X.J., Rice, F.L., Ernfors, P., 2011. Dependence on the transcription factor Shox2 for specification of sensory neurons conveying discriminative touch. Eur. J. Neurosci. 34, 1529–1541.

Abraira, V.E., Ginty, D.D., 2013. The sensory neurons of touch. Neuron 79, 618–639.

Alcaino, C., Knutson, K., Gottlieb, P.A., Farrugia, G., Beyder, A., 2017. Mechanosensitive ion channel Piezo2 is inhibited by D-GsMTx4. Channels 11, 245–253.

Baser, A., Skabkin, M., Kleber, S., Dang, Y., Balta, G.S.G., Kalamakis, G., Goepferich, M., Ibañez, D. C., Schefzik, R., Lopez, A.S., 2019. Onset of differentiation is post-transcriptionally controlled in adult neural stem cells. Nature 566, 100–104.

Bellier, J.P., Kimura, H., 2007. Acetylcholine synthesis by choline acetyltransferase of a peripheral type as demonstrated in adult rat dorsal root ganglion. J. Neurochem. 101, 1607–1618.

Bourane, S., Garces, A., Venteo, S., Pattyn, A., Hubert, T., Fichard, A., Puech, S., Boukhaddaoui, H., Baudet, C., Takahashi, S., 2009. Low-threshold mechanoreceptor subtypes selectively express MafA and are specified by Ret signaling. Neuron 64, 857–870.

Chambers, S.M., Qi, Y., Mica, Y., Lee, G., Zhang, X.-J., Niu, L., Bilsland, J., Cao, L., Stevens, E., Whiting, P., 2012. Combined small-molecule inhibition accelerates developmental timing and converts human pluripotent stem cells into nociceptors. Nat. Biotechnol. 30, 715–720.

Chesler, A.T., Szczot, M., Bharucha-Goebel, D., Čeko, M., Donkervoort, S., Laubacher, C., Hayes, L.H., Alter, K., Zampieri, C., Stanley, C., 2016. The role of PIEZO2 in human mechanosensation. N. Engl. J. Med. 375, 1355–1364.

Coleman, M. 2005. Axon degeneration mechanisms: commonality amid diversity. Nat. Rev. Neurosci. 6, 889–898.

Coste, B., Mathur, J., Schmidt, M., Earley, T.J., Ranade, S., Petrus, M.J., Dubin, A.E., Patapoutian, A., 2010. Piezo1 and Piezo2 are essential components of distinct mechanically activated cation channels. Science 330, 55–60.

Delmas, P., Hao, J., Rodat-Despoix, L.J.N.R.N., 2011. Molecular mechanisms of mechanotransduction in mammalian sensory neurons. Nat. Rev. Neurosci. 12, 139–153.

Dhandapani, R., Arokiaraj, C.M., Taberner, F.J., Pacifico, P., Raja, S., Nocchi, L., Portulano, C., Franciosa, F., Maffei, M., Hussain, A.F.J.N.C., 2018. Control of mechanical pain hypersensitivity in mice through ligand-targeted photoablation of TrkB-positive sensory neurons. Nat. Commun. 9, 1–14.

Drew, L.J., Wood, J.N., Cesare, P., 2002. Distinct mechanosensitive properties of capsaicin-sensitive and -insensitive sensory neurons. J. Neurosci., 22, RC228–RC228.

Du, X., Hao, H., Yang, Y., Huang, S., Wang, C., Gigout, S., Ramli, R., Li, X., Jaworska, E., Edwards, I., 2017. Local GABAergic signaling within sensory ganglia controls peripheral nociceptive transmission. J. Clin. Invest. 127, 1741–1756.

Ertürk, A., Hellal, F., Enes, J., Bradke, F., 2007. Disorganized microtubules underlie the formation of retraction bulbs and the failure of axonal regeneration. J. Neurosci., 27, 9169–9180.

Fernández-Trillo, J., Florez-Paz, D., Íñigo-Portugués, A., González-González, O., Del Campo, A. G., González, A., Viana, F., Belmonte, C., Gomis, A., 2020. Piezo2 mediates low-threshold mechanically evoked pain in the cornea. J. Neurosci. 40, 8976–8993.

García-Mesa, Y., García-Piqueras, J., García, B., Feito, J., Cabo, R., Cobo, J., Vega, J., García-Suárez, O., 2017. Merkel cells and Meissner's corpuscles in human digital skin display Piezo2 immunoreactivity. J. Anat. 231, 978–989.

Goto, T., Kuramoto, E., Dhar, A., Wang, R.P.-H., Seki, H., Iwai, H., Yamanaka, A., Matsumoto, S.-E., Hara, H., Michikawa, M., 2020. Neurodegeneration of trigeminal mesencephalic neurons by the tooth loss triggers the progression of Alzheimer's disease in 3× Tg-AD model mice. J. Alzheimer's Dis. 1–17.

Gudipaty, S.A., Lindblom, J., Loftus, P.D., Redd, M.J., Edes, K., Davey, C., Krishnegowda, V., Rosenblatt, J., 2017. Mechanical stretch triggers rapid epithelial cell division through Piezo1. Nature 543, 118–121.

Hao, J., Delmas, P., 2010. Multiple desensitization mechanisms of mechanotransducer channels shape firing of mechanosensory neurons. J. Neurosci. 30, 13384–13395.

Hu, J., Lewin, G.R., 2006a. Mechanosensitive currents in the neurites of cultured mouse sensory neurones. J. Physiol. 577, 815–828.

Iggo, A, Andres, K H, 1982. Morphology of cutaneous receptors. Ann. Rev. Neurosci. 5 (1), 1–31.

Jarvie, B.C., Hentges, S.T., 2012. Expression of GABAergic and glutamatergic phenotypic markers in hypothalamic proopiomelanocortin neurons. J. Comp. Neurol. 520, 3863–3876.

Jetta, D., Gottlieb, P.A., Verma, D., Sachs, F., Hua, S.Z., 2019. Shear stress-induced nuclear shrinkage through activation of Piezo1 channels in epithelial cells. J. Cell Sci. 132.

Johnson, J.A., Liu, H., Höger, U., Rogers, S.M., Sivapalan, K., French, A.S., Torkkeli, P.H. 2021. Mechanotransduction channel Piezo is widely expressed in the spider, Cupiennius salei, mechanosensory neurons and central nervous system. Sci. Rep., 11, 1–13.

Koschorke, G.-M., Meyer, R., Campbell, J.N., 1994. Cellular components necessary for mechanoelectrical transduction are conveyed to primary afferent terminals by fast axonal transport. Brain Res. 641, 99–104.

Lallemend, F., Ernfors, P., 2012. Molecular interactions underlying the specification of sensory neurons. Trends Neurosci. 35, 373–381.

Lechner, S.G., Lewin, G.R., 2013. Hairy sensation. Physiology 28, 142–150.

Lecoin, L., Rocques, N., El-Yakoubi, W., Achour, S.B., Larcher, M., Pouponnot, C., Eychène, A., 2010. MafA transcription factor identifies the early ret-expressing sensory neurons. Dev. Neurobiol. 70, 485–497.

Levanon, D., Bettoun, D., Harris-Cerruti, C., Woolf, E., Negreanu, V., Eilam, R., Bernstein, Y., Goldenberg, D., Xiao, C., Fliegauf, M., 2002. The Runx3 transcription factor regulates development and survival of TrkC dorsal root ganglia neurons. EMBO J. 21, 3454–3463.

Li, L., Rutlin, M., Abraira, V.E., Cassidy, C., Kus, L., Gong, S., Jankowski, M.P., Luo, W., Heintz, N., Koerber, H.R., 2011. The functional organization of cutaneous low-threshold mechanosensory neurons. Cell 147, 1615–1627.

Lu, H.-J., Nguyen, T.-L., Hong, G.-S., Pak, S., Kim, H., Kim, H., Kim, D.-Y., Kim, S.-Y., Shen, Y., Ryu, P.D., 2020. Tentonin 3/TMEM150C senses blood pressure changes in the aortic arch. J. Clin. Invest. 130, 3671–3683.

Matthes, S., Bader, M., 2018. Peripheral serotonin synthesis as a new drug target. Trends Pharmacol. Sci. 39, 560–572.

Mazzuoli-Weber, G., Kugler, E.M., Bühler, C.I., Kreutz, F., Demir, I.E., Ceyhan, O.G., Zeller, F., Schemann, M., 2019. Piezo proteins: incidence and abundance in the enteric nervous system. Is there a link with mechanosensitivity? Cell Tissue Res. 375, 605–618.

Miura, Y., Devaux, J.J., Fukami, Y., Manso, C., Belghazi, M., Wong, A.H.Y., Yuki, N., Group, C.-C.S., 2015. Contactin 1 IgG4 associates to chronic inflammatory demyelinating polyneuropathy with sensory ataxia. Brain 138, 1484–1491.

Narayanan, P., Sondermann, J., Rouwette, T., Karaca, S., Urlaub, H., Mitkovski, M.O., Gomez-Varela, D., Schmidt, M., 2016. Native Piezo2 interactomics identifies Pericentrin as a novel regulator of Piezo2 in somatosensory neurons. J. Proteome Res. 15, 2676–2687.

Naujock, M., Stanslowsky, N., Reinhardt, P., Sterneckert, J., Haase, A., Martin, U., Kim, K.-S., Dengler, R., Wegner, F., Petri, S., 2014. Molecular and functional analyses of motor neurons generated from human cord-blood-derived induced pluripotent stem cells. Stem Cells Dev. 23, 3011–3020.

Nickolls, A.R., Lee, M.M., Espinoza, D.F., Szczot, M., Lam, R.M., Wang, Q., Beers, J., Zou, J., Nguyen, M.Q., Solinski, H.J., 2020. Transcriptional programming of human mechanosensory neuron subtypes from pluripotent stem cells. Cell Rep. 30, 932–946. e7.

Nolano, M., Provitera, V., Crisci, C., Stancanelli, A., Wendelschafer-Crabb, G., Kennedy, W.R., Santoro, L., 2003. Quantification of myelinated endings and mechanoreceptors in human digital skin. Ann. Neurol. 54, 197–205.

Nolano, M., Provitera, V., Estraneo, A., Selim, M.M., Caporaso, G., Stancanelli, A., Saltalamacchia, A.M., Lanzillo, B., Santoro, L., 2008. Sensory deficit in Parkinson's disease: evidence of a cutaneous denervation. Brain 131 (7), 1903–1911.

Orefice, L.L., Zimmerman, A.L., Chirila, A.M., Sleboda, S.J., Head, J.P., Ginty, D.D., 2016. Peripheral mechanosensory neuron dysfunction underlies tactile and behavioral deficits in mouse models of ASDs. Cell 166, 299–313.

Paek, K.Y., Hong, K.Y., Ryu, I., Park, S.M., Keum, S.J., Kwon, O.S., Jang, S.K., 2015. Translation initiation mediated by RNA looping. Proc. Natl. Acad. Sci. 112, 1041–1046.

Rajamani, U., Gross, A.R., Hjelm, B.E., Sequeira, A., Vawter, M.P., Tang, J., Gangalapudi, V., Wang, Y., Andres, A.M., Gottlieb, R.A., 2018. Super-obese patient-derived iPSC hypothalamic neurons exhibit obesogenic signatures and hormone responses. Cell Stem Cell 22, 698–712. e9.

Ranade, S.S., Woo, S.-H., Dubin, A.E., Moshourab, R.A., Wetzel, C., Petrus, M., Mathur, J., Bégay, V., Coste, B., Mainquist, J., 2014. Piezo2 is the major transducer of mechanical forces for touch sensation in mice. Nature 516, 121–125.

Ray, P., Torck, A., Quigley, L., Wangzhou, A., Neiman, M., Rao, C., Lam, T., Kim, J.-Y., Kim, T.H., Zhang, M.Q., 2018. Comparative transcriptome profiling of the human and mouse dorsal root ganglia: an RNA-seq-based resource for pain and sensory neuroscience research. Pain 159 (7), 1325–1345.

Reinhardt, P., Glatza, M., Hemmer, K., Tsytsyura, Y., Thiel, C.S., Höing, S., Moritz, S., Parga, J.A., Wagner, L., Bruder, J.M., 2013. Derivation and expansion using only small molecules of human neural progenitors for neurodegenerative disease modeling. PLoS One, 8, e59252.

Roh, J., Hwang, S.-M., Lee, S.-H., Lee, K., Kim, Y.H., Park, C.-K., 2020. Functional expression of Piezo1 in Dorsal root ganglion (DRG) neurons. Int. J. Mol. Sci. 21, 3834.

Rugiero, F., Drew, L.J., Wood, J.N., 2010. Kinetic properties of mechanically activated currents in spinal sensory neurons. J. Physiol. 588, 301–314.

Saito-Diaz, K., Street, J.R., Ulrichs, H., Zeltner, N., 2021. Derivation of peripheral nociceptive, mechanoreceptive, and proprioceptive sensory neurons from the same culture of human pluripotent stem cells. Stem Cell Rep. 16, 446–457.

Satoh, K., Hata, M., Takahara, S., Tsuzaki, H., Yokota, H., Akatsu, H., Yamamoto, T., Kosaka, K., Yamada, T., 2006. A novel membrane protein, encoded by the gene covering KIAA0233, is transcriptionally induced in senile plaque-associated astrocytes. Brain Res. 1108, 19–27.

Schrenk-Siemens, K., Wende, H., Prato, V., Song, K., Rostock, C., Loewer, A., Utikal, J., Lewin, G.R., Lechner, S.G., Siemens, J., 2015. PIEZO2 is required for mechanotransduction in human stem cell–derived touch receptors. Nat. Neurosci. 18, 10–16.

Sherriff, F., Bridges, L., Gentleman, S., Sivaloganathan, S., Wilson, S., 1994. Markers of axonal injury in post mortem human brain. Acta Neuropathol. 88, 433–439.

Silver, B.B., Wolf, A.E., Lee, J., Pang, M.-F., Nelson, C.M., 2020. Epithelial tissue geometry directs emergence of bioelectric field and pattern of proliferation. Mol. Biol. Cell, mbc. E19-12-0719.

Song, Y., Li, D., Farrelly, O., Miles, L., Li, F., Kim, S.E., Lo, T.Y., Wang, F., Li, T., Thompson-Peer, K.L.J.N., 2019. The mechanosensitive ion channel Piezo inhibits axon regeneration. Neuron 102, 373–389.

Specht, L.A., Pickel, V.M., Joh, T.H., Reis, D.J., 1981. Light-microscopic immunocytochemical localization of tyrosine hydroxylase in prenatal rat brain. I. Early ontogeny. J. Comp. Neurol. 199, 233–253.

Syeda, R., Florendo, M.N., Cox, C.D., Kefauver, J.M., Santos, J.S., Martinac, B., Patapoutian, A., 2016. Piezo1 channels are inherently mechanosensitive. Cell Rep. 17, 1739–1746.

Syeda, R., Xu, J., Dubin, A.E., Coste, B., Mathur, J., Huynh, T., Matzen, J., Lao, J., Tully, D.C., Engels, I.H., 2015. Chemical activation of the mechanotransduction channel Piezo1. Elife 4, e07369.

Szczot, M., Pogorzala, L.A., Solinski, H.J., Young, L., Yee, P., le Pichon, C.E., Chesler, A. T., Hoon, M.A., 2017. Cell-type-specific splicing of Piezo2 regulates mechanotransduction. Cell Rep. 21, 2760–2771.

Tamm, E.R., Flügel, C., Stefani, F.H., Lütjen-Drecoll, E., 1994. Nerve endings with structural characteristics of mechanoreceptors in the human scleral spur. Invest. Ophthal. Vis. Sci. 35, 1157–1166.

Tchieu, J., Zimmer, B., Fattahi, F., Amin, S., Zeltner, N., Chen, S., Studer, L., 2017. A modular platform for differentiation of human PSCs into all major ectodermal lineages. Cell Stem Cell 21, 399–410. e7.

Tomchek, S.D., Dunn, W., 2007. Sensory processing in children with and without autism: a comparative study using the short sensory profile. Am. J. Occup. Ther. 61, 190–200.

Usoskin, D., Furlan, A., Islam, S., Abdo, H., Lönnerberg, P., Lou, D., Hjerling-Leffler, J., Haeggström, J., Kharchenko, O., Kharchenko, P.V., 2015. Unbiased classification of sensory neuron types by large-scale single-cell RNA sequencing. Nat. Neurosci., 18, 145–153.

Wang, J., La, J.H., Hamill, O.P., 2019. Piezo1 is selectively expressed in small diameter mouse DRG neurons distinct from neurons strongly expressing TRPV1. Front. Mol. Neurosci. 12, 178.

Wang, Y., Chi, S., Guo, H., Li, G., Wang, L., Zhao, Q., Rao, Y., Zu, L., He, W., Xiao, B., 2018. A lever-like transduction pathway for long-distance chemical-and mechano-gating of the mechanosensitive Piezo1 channel. Nat. Commun. 9, 1–12.

Wende, H., Lechner, S.G., Cheret, C., Bourane, S., Kolanczyk, M.E., Pattyn, A., Reuter, K., Munier, F.L., Carroll, P., Lewin, G.R., 2012. The transcription factor c-Maf controls touch receptor development and function. Science 335, 1373–1376.

Woo, S.-H., Ranade, S., Weyer, A.D., Dubin, A.E., Baba, Y., Qiu, Z., Petrus, M., Miyamoto, T., Reddy, K., Lumpkin, E.A., 2014. Piezo2 is required for Merkel-cell mechanotransduction. Nature 509, 622–626.

Yang, N., Chanda, S., Marro, S., Ng, Y.-H., Janas, J.A., Haag, D., Ang, C.E., Tang, Y., Flores, Q., Mall, M., 2017. Generation of pure GABAergic neurons by transcription factor programming. Nat. Methods 14, 621–628.

Yao, M., Tijore, A.S., Cox, C.D., Hariharan, A., Van Nhieu, G.T., Martinac, B., Sheetz, M., 2020. Force-dependent Piezo1 recruitment to focal adhesions regulates adhesion maturation and turnover specifically in non-transformed cells. bioRxiv.

Zhang, M., Wang, Y., Geng, J., Zhou, S., Xiao, B., 2019. Mechanically activated piezo channels mediate touch and suppress acute mechanical pain response in mice. Cell Rep. 26, 1419–1431. e4.

Zhang, T., Chi, S., Jiang, F., Zhao, Q., Xiao, B., 2017. A protein interaction mechanism for suppressing the mechanosensitive Piezo channels. Nat. Commun. 8, 1–13.

Zhu, S., Zhao, C., Wu, Y., Yang, Q., Shao, A., Wang, T., Wu, J., Yin, Y., Li, Y., Hou, J., 2015. Identification of a Vav2-dependent mechanism for GDNF/Ret control of mesolimbic DAT trafficking. Nat. Neurosci. 18, 1084–1093.

Zurborg, S., Piszczek, A., Martínez, C., Hublitz, P., Banchaabouchi, M.A., Moreira, P., Perlas, E., Heppenstall, P.A., 2011. Generation and characterization of an Advillin-Cre driver mouse line. Mol. Pain 7, 1744–8069-7-66.